Modeling of Heat Transfer during Combustion: A Quasi-Dimensional Approach with Emphasis on Large Low-Speed Diesel Engines

K.Boulouchos and R.Isch

Swiss Federal Institute of Technology
ETH-Zentrum
CH-8092 Zürich
Switzerland

ABSTRACT

A model for predicting heat transfer rates to the combustion chamber walls of diesel engines is presented. The algorithm treats both convection and radiation as mechanisms of equal importance and uses appropriate submodels for key parameters like flame and zonal gas temperatures, turbulence quantities, area view factor and soot cloud emissivity. Aspects of chamber geometry, intake and injection configurations can be accounted for in this way, though in a simplified manner. Predictions for spatially averaged heat fluxes are given, but the model framework permits calculations of local parameters also. Emphasis is put into large, low-speed engines but the adaptation for smaller, medium and high speed diesel engines is straight forward. Comparisons with available experimental data have been performed, demonstrating an extended ability to predict heat transfer behaviour in a wide range of engine operating conditions as compared to existing global, zero-dimensional models. Results of parametric sensitivity studies underline thereby the physical consistence of the model.

INTRODUCTION

In-cylinder heat transfer is an issue of growing interest within the engine research community for several reasons. First, heat losses from the cylinder contents to the wall affect the thermodynamic efficiency of the energy conversion process. In addition the local wall heat flux is to a significant extent responsible for the surface temperature level and hence for tribological behaviour and durability of the combustion chamber confinement, in particular for the cylinder liner ([1]). Furthermore reaction kinetics governing pollutant formation and knock occurrence are usually strongly dependent on species temperature, which generally varies widely over space and time within the combustion chamber. Recently the controversy about the origin of the observed enhancement of heat transfer rates in the case of so-called adiabatic or low-heat rejection engines concepts ([2]) added to the motivation for exploring the I.C. engines heat transfer process in even more detail and depth.
A very informative survey concerning measurement techniques, correlations and application in practical engines can be found in [3] and an excellent review with updated information on fundamental questions is given in [4].

Early experimental work on engine heat transfer dates back to 1939 and led to the well known Eichelberg equation ([5]). Subsequently global zero-dimensional correlations have been proposed, some taking into account the different physics of convection and radiation ([6],[7]), while others ([8],[9]) lump the second mechanism in a single term together with the general enhancement of wall heat flux due to combustion. Woschni's equation for the spatially averaged heat transfer coefficient ([9]) has been widely accepted during the last 20 years, mainly due to its simplicity and physical consistence, the latter being valid only for the convection mechanism, whose calculation is based on steady state Reynolds analogy. Sometimes also the approach of Annand ([7]) has been considered. Nevertheless, all these correlations can at best only fit heat balance trends over a limited range of operating conditions and they generally fail to reproduce quantitatively even global heat transfer behaviour for different engine geometries and sizes. Moreover they lack the ability to incorporate the influence of design parameters like injection configuration, intake and combustion chamber geometry etc.
On the other end of the spectrum, multidimensional models would theoretically allow to account for flow field features in sufficient spatial and temporal resolution, in particular for the evolution of the compressible thermal turbulent layer at the cylinder walls. Related state of the art models however are almost without exception based on the so called universal law of the wall, whose relevance for unsteady three dimensional engine flows must be strongly questioned ([10]). Furthermore distribution and structure of reaction sheets and their interaction with the flow field clearly cannot be reliably described on a fundamental basis at the current state of knowledge, so that multidimensional modeling has also to work with crude phenomenological assumptions in this context. In addition, the required computer time and diagnostic tools are scarcely affordable by the majority of industrial development groups.
Indeed a new class of "intermediate" models has evolved during the last decade ([11], [12], [13], [14], [15]), which attempt to describe heat transfer behaviour mainly on a phaenomenological basis. However, they incorporate some details of the flow field contribution to convection and/or radiation physics and, though being essentially zonal models, they often reproduce engine heat transfer remarkably well.

The objective of the work presented here is to develop an improved physically consistent but simplified and thus, affordable, user-transparent algorithm for predicting heat transfer behaviour in a variety of operating conditions and design parameters. The development work thereby has been based on preliminary modeling efforts [15] and on an extended experimental data-set ([16]) of heat flux and energy balance analysis as well as on gas and flame temperatures together with local LDV-measurements in a large, low speed, two-stroke diesel engine.

The following section describes the physical basis and the equations used in the model. The methodology of matching and comparison to engine data as well as relevant operating conditions are then presented. Next, the results obtained from calculations, including parametric and sensitivity studies are presented and discussed. Finally, the conclusions reached so far are summarized and an outlook for proposed future investigations is given.

MODEL DESCRIPTION

The basic assumptions leading to the algorithm formulation will be presented in this section and the relevant equations are shown in Table 1.

The total heat flux is thought for this engine size to consist of both convection and radiation (Eq.(1)). Thus Eq. (2) for the heat transfer coefficient is only a formal description without exact physical meaning, since radiation is not driven by a characteristic temperature difference. The approach for calculating the radiative part of the heat flux (in the following to be understood as an instantaneous spatially averaged quantity) includes a procedure for computing the area view factor between combustion chamber wall and soot cloud, the characteristic radiation temperature and the emissivity of the soot zone. For the emissivity of the wall, approximate values based on experience ([3]) have been used, whereas the piston-covered part of the cylinder liner was distinguished from the chamber surface still exposed to combustion at TDC. In all others but a few extreme low heat rejection designs, the wall temperature contribution to Eq. (3) is not significant and may be neglected.

The temporal behaviour of the area view factor is thought to reflect the penetration of the injected spray into the combustion chamber (Eqs. (4) through (7)), the underlying assumption being that radiating soot particles are distributed mostly in the inner side of the spray cone. Spray tip penetration and cone angle correlations are averages of equations for turbulent jets proposed by various authors. The formulation for the spatially averaged area view factor (Eq.(4)) is not arbitrary, but has its origin in a detailed computation of instantaneous local values based on a finite element scheme ([17]); the parameters C_1 and C_2 are then matched so as to be representative for the integral value of the area view factor.

The effective radiation temperature is very difficult to estimate with reasonable accuracy. Moreover its influence on the resulting heat flux is due to the fourth-power law enormous. Eq.(8) yields the radiation temperature as a weighted average between the energetically mean temperature of the fluid and the theoretically achievable highest process temperature, namely the one prevailing in thin, stoechiometric diffusion reaction zones, under mainly adiabatic conditions. The latter temperature is computed simply through Eq. (11), while for the instantaneous mean process temperature reliable data of either the heat release rate or the cylinder pressure are necessary. Since for computing the convective heat flux both temperatures of the overall burned and unburned zone are each time needed, in principle a three-zone approximation is used in the algorithm. Each zone temperature is calculated based on anappropriate Viebe-function corresponding to the measured heat release rate for the process investigated.

The weighting factors for the interpolation in Eq. (8) are given in Eqs. (9) and (10). Though Eq. (9) has been derived through matching measured values of radiation temperatures at two distinct engine processes (s. next section), a certain physical interpretation can be given to its form. The influence of the burned mass fraction namely can be explained by the fact, that as combustion progresses much more earlier produced soot exists in the cooler surroundings of the flame, than in the instantaneously burning reaction zone. The sharp drop of the radiation temperature towards the mean process temperature close to or after the end of combustion has been observed experimentally by several authors ([3]). On the other side, with more excess air, oxidation rates of soot are higher, so that the soot formed in the primary burning zone contributes more to the radiation temperature, than the smaller amount of survived soot, formed in earlier stages of combustion; thus the influence of equivalence ratio on the weighting factors (mainly through the denominator of Eq. (9)) can also be understood at least in a qualitative sense.

As for soot emissivity, an approach given in [13] has been adapted in the model presented here (Eqs. (12) through (18)). Other correlations from various authors ([18]) give very similar emissivity results, though the predicted instantaneous soot volume fractions differ widely from each other. Obviously this can be attributed to the dominating influence of combustion chamber size on the soot emissivity (s.Eq. (12)). Nevertheless for smaller diesel engines the effect of different correlations for soot production and oxidation might be far more important than in the present case and has to be evaluated carefully.

A general description of the convective part of heat flux is given in Eq. (20). Essentially Reynolds analogy is used, but instead of mean piston velocity and cylinder bore a characteristic turbulence intensity together with an associated length scale are computed for each turbulence generator during compression, combustion and expansion. The intake flow, the fuel injection and the secondary flow arising from density differences across the cylinder radius under high swirl during combustion ([16]) are considered as separate turbulence generators. Originally a very simplified balance equation for turbulent kinetic energy during intake and compression (subscript: motor) has been used, but in a later stage Eq. (21) was incorporated. This equation uses meanwhile LDA-data available during compression and expansion (but not during combustion) for the turbulence intensity and an argument based on rapid compression of turbulent eddies for the integral length scale. Eq. (22) reflects the influence of swirl number on turbulence intensity at Bottom Dead Center somewhat arbitrarily, but for the moment there does

Table 1: Equations used in the model

$$\dot{q}_{w,tot} = \dot{q}_{w,conv} + \dot{q}_{w,Rad} \quad (1) \quad , \quad \alpha_{tot} = \dot{q}_{w,tot} / (T_m - T_w) \quad (2)$$

$$\dot{q}_{w,Rad} = \varepsilon_w \cdot \varepsilon_s \cdot \psi_{s,w} \cdot (T_{Rad}^4 - T_w^4) \quad (3)$$

$$\psi_{s,w} = C_1 \cdot (1 - \exp(-C_2 \cdot A_{spr}/A_p)) \quad (4)$$

$$A_{spr}/A_p = 8 \cdot \tan(\theta/2) \cdot (x/D)^2 \quad (5)$$

$$x = (13{,}8 \cdot U_{inj} \cdot \delta \cdot t)^{0.5} \quad (6) \quad , \quad U_{inj} = (2 \cdot \Delta p_{inj}/\rho_f)^{0.5} \quad (7)$$

$$T_{Rad} = f_1 \cdot T_{f,ad} + f_2 \cdot T_m \quad (8) \quad , \quad f_1 = \frac{(1-\xi)^{\lambda^{-2}}}{1 + 1{,}4 \cdot \lambda^{-2}} \quad (9)$$

$$f_2 = 1 - f_1 \quad (10) \quad , \quad T_{f,ad} = H_u/\bar{c}_p + T_u \quad (11)$$

$$\varepsilon_s = 1 - \exp\{-1575 \cdot f_v \cdot \ell_s \cdot T_{Rad}\} \quad (12)$$

$$\ell_s = D \cdot \left(\frac{3}{16} \cdot \frac{H/D}{V_H/V(\varphi)}\right)^{1/3} \quad (13) \quad , \quad f_v = (m_s/\rho_s)/V(\varphi) \quad (14)$$

$$\dot{m}_s = \dot{m}_{s,fo} - \dot{m}_{s,b} \quad (15)$$

$$\dot{m}_{s,fo} = A_1 \cdot \dot{m}_{b,fu} \cdot \exp(-A_2/T_b) \quad (16) \quad , \quad \dot{m}_{b,fu} = \dot{\xi} \cdot m_{fu,tot} \quad (17)$$

$$\dot{m}_{s,b} = -B_1 \cdot \dot{m}_s/(\rho_s d_s) \cdot \exp(-B_2/T_{Rad}) \cdot p_{O_2}^{0.5} \quad (18)$$

$$p_{O_2} = p_{cyl.} \cdot \{0.49 + (\lambda - 1)/5.06\} \quad (19)$$

$$\dot{q}_{conv} = 400 \cdot C_3 \cdot p_{cyl}^{0.8} \left\{ \sum_i (u_i'^{0.8} \cdot L_i^{-0.2}) \cdot \sum_K \frac{A_{i,K}}{A_{tot}} \cdot (T_K - T_W) \cdot \left(\frac{T_K + T_W}{2}\right)^{-0.5} \right\}$$

i = motor, inj, sec.flow / K = burned, unburned (20)

$$u'^{0.8} \cdot L^{-0.2}\Big|_{motor} = \left\{ \frac{u'_{BDC}}{} \cdot (1 - 0.3\,\frac{\varphi - 180}{180}) \right\}^{0.8} \cdot \left\{ \frac{1}{2} h_{port} \cdot (V_{BDC}/V(\varphi))^{1/3} \right\}^{-0.2} \quad (21)$$

$$u'_{BDC} = \left\{ \left(\frac{1 + C_4 \cdot (z_{SW}/4)^2}{2} \right)^{0.5} \right\} \cdot \bar{u}_p \quad (22)$$

$$u'^{0.8} \cdot L^{-0.2}\Big|_{inj} = 1{,}33 \cdot U_{inj} \cdot \delta^{0.3} \cdot t^{-0.5} \quad (23)$$

$$u'^{0.8} \cdot L^{-0.2}\Big|_{sec.flow} = \left\{ 0{,}2 \cdot \bar{u}_p \cdot z_{SW}/4 \cdot (\alpha \varphi_{asi}^2 + \beta \varphi_{asi}) \right\}^{0.8} \cdot \left(\frac{\bar{h}_{cc}}{20}\right)^{-0.2} \quad (24)$$

$$\alpha = -4 \cdot \Phi^{-2} \quad (25) \quad , \quad \beta = 4 \cdot \Phi^{-1} \quad (26) \quad , \quad \Phi^{-1} = \frac{z_{SW}/4}{30 + \varphi_{ei} \cdot z_{SW}/4} \quad (27)$$

$$A_{motor} = A_{tot} \quad , \quad A_{inj} = 2 \cdot \tan(\theta/2) \cdot x^2 \quad , \quad A_{sec.flow} = 2 \cdot A_p \quad (28)$$

Piston and cylinder head: $\Rightarrow$ Eq. (29)

Cylinder liner: $\Rightarrow$ Eq. (30)

$$\frac{A_{i,b}}{A_i} = \frac{(V_b/V_u)^{2/3}}{1 + (V_b/V_u)^{2/3}} \quad (29) \qquad \frac{A_{i,b}}{A_i} = \frac{(V_b/V_u)^{2/3}}{1 + (V_b/V_u)^{2/3}} \cdot (1 - \eta) \quad (30)$$

i = motor, sec.flow, inj. $\qquad$ i = motor, inj.

$$\left.\begin{array}{l} \varphi < \varphi_{si} : \eta = 0 \quad , \quad \varphi > 120/z_{SW} + \varphi_{ei} : \eta = 1 \\ \varphi_{si} \leq \varphi \leq 120/z_{SW} + \varphi_{ei} : \eta = \dfrac{z_{SW}/4 \cdot (\varphi - \varphi_{si})}{30 + \frac{z_{SW}}{4} \cdot (\varphi_{ei} - \varphi_{si})} \end{array}\right\} \quad (31)$$

$\rho_s = 1000\ kg/m^3$, $d_s = 1 \cdot 10^{-7}\ m$

not exist a reliable experimental basis for a better correlation. Eqs. (23) through (27) describe the convective parameter of interest for the other two turbulence generators. For the case of the swirl-induced secondary flow during combustion a simplified calculation for the order of magnitude of the radial velocity in analogy to free convection driven by density differences has been used.

Finally, Eqs. (28) to (31) yield the actual surface area, on which each turbulence generator acts. Eq.(29) refers to cylinder head and piston, while Eq. (30) refers to the cylinder liner. The distribution of cold and hot zones in dependence of the corresponding volumes, the latter being derived by the heat release rate, is of course only an approximation. Of particular interest in this context is the assumed linear transition of the fluid temperature in the neighbourhood of the cylinder liner from "hot" to "cold" based on Eqs. (30) and (31).

ENGINE DATA

The model described in the previous section has been systematically tested against a well documented engine data set in order to assess its ability to predict heat transfer behaviour over a variety of engine operating conditions. Table 2 summarizes the main characteristics of the large, low-speed diesel engine under consideration.

Table 2: Principal engine data

Bore:	560 mm	Intake:	Swirl ports
Stroke:	1400 mm	Exhaust:	Single central exhaust valve
Compr. Ratio: or 20.5	17.7	Geometry:	Swirl number 4 no squish

The standard injection configuration consists of three injection nozzles, each equipped with five holes. The nozzles are located in the periphery of the cylinder head and are 120° apart from each-other in circumferential direction.

The operating conditions used for comparison have been chosen so as to include a for this type of engine relatively wide range of speeds, loads and extents of supercharging. The key operating conditions selected for evaluating the model performance are listed in Table 3.

Table 3: Engine operating conditions

Condition (Process)	1	2	3	4
Engine speed (rpm)	150	150	119	94.5
BMEP (bar)	15.5	15.5	9.75	6.15
Equiv. ratio	0.49	0.64	0.43	0.41
Relative power output	100	100	50	25

Operating condition 1 will be called "Reference Process" in the following, since it has been used to match the model set of constants, which of course remained then unchanged for the other conditions. For processes 1 and 2 the experimental data set is very detailed and includes also measurements of fluid velocity, heat flux, gas and flame temperature at a certain location of the combustion chamber ([16]). For all conditions cylinder pressure, heat release pattern and an integral energy balance analysis of the engine process are available. Thus the integral heat losses to the cylinder walls have been also determined.

The "Reference Process" corresponds also to full-load operation, while the condition 2 is thought to represent a characteristic process, towards which future engine development will presumably move in view of requirements for high specific power output and low investment cost for marine and stationary applications. Conditions 3 and 4 are derived from full load according to propeller-law.

In the following section results of calculations based on the described model are presented and discussed for all operating conditions.

RESULTS AND DISCUSSION

The new algorithm has been applied to the selected engine operating conditions and the results have been compared with experimental data as well as with predictions based an the correlations proposed by Woschni, Annand and Eichelberg. All these models refer to the high pressure part of the engine cycle, i.e. compression, combustion and expansion. Thus, comparisons with measured energy balance trends rely on the assumption, that for the same engine the ratio of heat losses during the gas exchange process to the total heat losses is for the considered operating conditions roughly constant. Experimental evidence exists, that in the considered cases this ratio has approximately the value 0.1. Furthermore the main constants for the new algorithm and for the models used for comparison, have been scaled so as to match the experimental results at the Reference Operating Condition (Process 1). The set of constants has then been kept unchanged for all processes so that a fair comparison of performance between all models can be carried through. Table 4 shows the resulting values of the constants used in our model (ETH) and the scaling factors for the other three correlations.

Table 4: Set of constants and scaling factors

(a) ETH-model:

C_1=0.70 , C_2=7.3 , C_3=0.295 , C_4=1.0

(b) Scaling-factor:

Woschni: 0.64 , Annand: 0.58 , Eichelberg: 0.57

Results of calculations, comparisons with measurements and parametric sensitivity studies are then as follows:

Fig. 1 shows soot emissivity and area view factor for processes 1 and 3 over crankangle. The soot cloud is optically thick during combustion mainly due to the large engine size, while the area view factor peaks around the end of injection (20 deg CA). Radiation temperatures for processes 1 through 4 are shown in Fig. 2. It is interesting to notice the actually small deviations of peak level for all processes, a fact that has been experimentally observed also for smaller, high speed diesel engines.
Fig. 3 shows a comparison between measured and calculated radiation temperatures for processes 1 and 2. A satisfactory agreement can be claimed in particular for the mid-phase of combustion, where both area view factor and radiation temperature have high values and hence the contribution of radiation to the total heat flux is important.

Shown in Fig. 4 and 5 are the contributions of all turbulence generators to the convective heat flux for processes 1 and 3. The enhancement of convection due to combustion is obviously significant and has to be taken into account.
From Fig. 6 it is obvious that radiation and convection are of similar importance as far as it concerns the integral heat losses to the walls. The slight redistribution towards more radiation for low load is due to the influence of lower engine speeds (propeller-law!) on the convective heat flux. A direct comparison of Woschni's proposal with the ETH-model for the Reference process is displayed in Fig. 7. Deviations of heat transfer coefficient values between various models in the early combustion phase are of minor importance in terms of heat fluxes and heat losses as stated by Figs. 8,9 and 10. These diagrams compare heat fluxes (Fig. 8) and heat losses (Fig. 9) for the Reference process as well as heat fluxes for process 3 (Fig. 10), all calculated according to the present model and to the correlations of Woschni, Annand and Eichelberg. More severe implications for the accuracy of predictions has the later part of combustion and the early expansion phase where both spatially averaged temperatures and total heat exchange surface area have high values.
In any case, Figs. 8 through 10 display similar predictions on one side by the approach of Woschni and of the present model and on the other side by the correlations of Annand and Eichelberg. The two subgroups exhibit then clearly a different behaviour from each other. Since all four models differ widely in terms of physical relevance for convection and/or radiation, the observed similarities may be in part fortitious at least for these engine operating conditions.

However, the key diagram for a comparative evaluation of model performance is certainly Fig. 11. For all operating conditions the best performance is clearly achieved by the model described in the present work. Woschni's results may be viewed to a certain degree as acceptable, while the agreement of the other two correlations with experimental values is rather poor.

Additional advantages of the new algorithm are demonstrated in Figs. 12 and 13. Shown here is the ability to account for changes of important design parameters like swirl intensity and injection configuration. The basic assumption for these

extrapolations however is that the heat release rate is not significantly affected by such design modifications, simply because the correct heat release pattern is usually not known in advance. As for the difference in the two curves of Fig. 13, the explanation is given by the major and combined influence of higher injection pressures on both turbulence enhancement and increase rate of area view factor.

It is informative also to look at sensitivity trends as displayed by Figs. 14 and 15. Obviously the constants C_1 and C_3 are the most important ones, while the influence of C_2 and C_4 (the latter not shown here) is, as expected, very small, at least for general purposes, i.e. if only integrated total heat losses are of interest.

CONCLUSIONS:

A model for predicting heat transfer rates in diesel engines has been developed and tested extensively on the basis of a detailed experimental data set including measurements of overall energy balance, local heat flux, gas temperature within the turbulent boundary layer, local flow field quantities and spatially averaged flame temperature in a large, low-speed, two stroke direct injection diesel engine. The model treats both convection and radiation as equally important mechanisms and uses phaenomenological submodels for a few basic parameters like three-zone-temperatures, area view factor and soot emissivity as well as characteristic length scales and fluctuation intensities corresponding to each turbulence generator in the combustion chamber.

The following conclusions were reached:

1. The algorithm corresponds to experimentally observed trends of integral heat losses to the cylinder walls over a for this type of engine wide range of speeds and loads with quantitative accuracy and far better than any of the currently well accepted zero dimensional engine heat transfer models. The same set of constants has been thereby used for all conditions after an initial matching based on a selected reference process of the engine.

2. Radiation and convection contribute for all considered conditions with roughly equal parts to the total spatially averaged heat flux to the combustion chamber walls. The fuel injection configuration emerges as a significant parameter for both processes, due to its influence first on local turbulence enhancement and second on the evolution of the area view factor over time.

3. Although emphasis has been put on spatially averaged behaviour in large low speed diesel engines, the physical basis and structure of the model allows a straight-forward extension to either local heat fluxes or to smaller size, medium to high speed diesel engines.

4. Parametric studies demonstrate the ability of the algorithm at the current stage of development to predict the response of heat losses to modifications of major design parameters, like injection pressure, nozzle configuration and swirl intensity.

Future work will include adaptation of the model to smaller, four-stroke diesel engines with non-quiescent combustion chambers characterized also by moderate to strong squish. For this purpose it is intended to generate an as complete as possible experimental data set in a single cylinder research engine of appropriate size and geometry.

NOMENCLATURE:

q: wall heat flux
T: temperature
z_{sw}: swirl number
A: surface area
u,U: velocity
u': turbulence intensity
L: integral length scale of turbulence
h: height
H: stroke
D: bore
d: diameter
$\bar{c}_p$: average thermal capacity
Hu: heat of reaction of stoechiometric mixture
V: volume
f_v: volume fraction
l_s: average thickness of soot zone
x: spray tip penetration

Greek:

α: heat transfer coefficient
ε: emissivity
ψ: area view factor
θ: half-angle of spray cone
φ: crankangle
λ: reciproce of equivalence ratio
δ: nozzle orifice diameter
ρ: density
ξ: dimensionles burned mass fraction

Subscripts

w: wall
s: soot
b: burned
u: unburned
fo: formed
fu: fuel
p: piston
si: start of injection
asi: after start of injection
ei: end of injection

ACKNOWLEDGEMENTS

The authors wish to acknowledge the contribution of Sulzer Diesel Co. to this work, which provided several experimental data of engine processes relevant for comparison with the model. Prof. M.K. Eberle is also thanked for his encouragement and active support of the project.

REFERENCES

[1]: Eberle, M.K.: "Diesel Engine Design for Reliability, Cost Effectiveness and Environmental Acceptability - An Outlook", 1990 Calvin Rice Lecture, ASME.

[2]: Woschni, G., Spindler, W.: "Heat Transfer with Insulated Combustion Chamber Walls and its Influence on the Performance of Diesel Engines", 11th. Ann., Energy-Sources Techn. Conf. and Exhib., New Orleans, Louisianna, 1988.

[3]: Mollenhauer, K., Pflaum, W.:"Wärmeübergang in der Verbrennungskraftmaschine", Springer Verlag, Wien - New York, 1977.

[4]: Borman, G., Nishiwaki, K.: "Internal Combustion Engine Heat Transfer", Progr. Energy Combust. Sci. 1987, Vol. 13, pp. 1-46.

[5]: Eichelberg, G.: "Some new investigations on old combustion-engine problems", Engineering (148), London, 1939.

[6]: Sitkei, G.:"Beitrag zur Theorie des Wärmeübergangs im Motor", Konstruktion 14, 67-71(1962).

[7]: Annand, W.J.D.: "Heat Transfer in the Cylinder of Reciprocating Internal Combustion Engines", Inst. of Mech.Eng., London, 1963.

[8]: Elser, K.: "Der instationäre Wärmeübergang in Dieselmotoren", Mitteilungen aus dem Institut für Thermodynamik und Verbrennungsmotorenbau, ETH Zürich, 1954, Nr. 15.

[9]: Woschni, G.: "Die Berechnung der Wandverluste und der thermischen Belastung der Bauteile von Dieselmotoren", MTZ (31), 1970.

[10]: Gosman, A.D.: "Computer Modelling of Flow and Heat Transfer in Engines, Progress and Prospects", COMODIA 1985, Tokyo, JSME.

[11]: Chapman, M., Friedman, M.C., Aqhan, A.: "A Time-Dependent Spatial Model for Radiant Heat Transfer in Diesel Engines", SAE Paper 83125, 1983.

[12]: Morel, T., Keribar, R.: "A Model for Predicting Spatially and Time Resolved Convective Heat Transfer in Bowl-in Piston Combustion Chambers", SAE Paper 850204, 1985.

[13]: Morel, T., Keribar, R.: "Heat Radiation in D.I. Diesel Engines", SAE Paper 860445, 1986.

[14]: Poulos, S.G., Heywood, J.B.: "The effect of chamber geometry on spark-ignited engine combustion", SAE Paper 830334 (1983).

[15]: Boulouchos, K., Hannoschöck, N.: "Der Wärmetransport zwischen Arbeitsmedium und Brennraumwand", Motortechnische Zeitschrift MTZ (47), 1986.

[16]: Boulouchos, K., Eberle, M.K., Ineichen, B., Klukowski, C.: "New Insights into the Mechanisms of In-Cylinder Heat Transfer in Diesel Engines", SAE Paper 890573, 1989.

[17]: Brunner, D.: "Berechnung der Wärmestrahlung im Dieselmotor unter besonderer Berücksichtigung des Raumwinkelverhältnisses", Diplomarbeit, Inst. f. Energietechnik, ETH Zürich, 1988.

[18]: "Particulate Carbon Formation During Combustion", GM Res.Labs., Plenum Press, 1981.

FIGURES

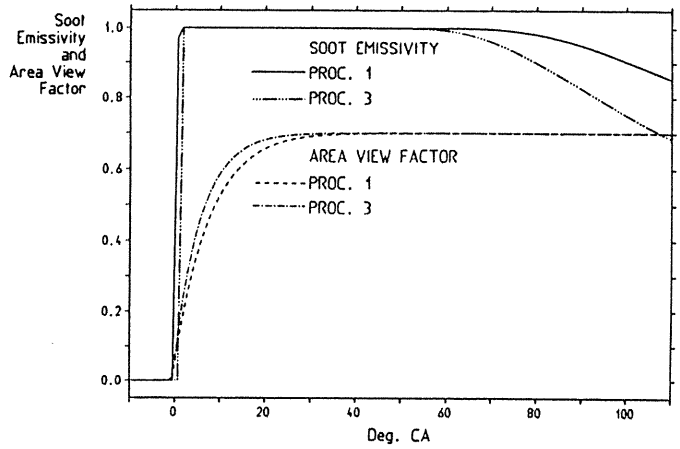

Fig. 1: Soot emissivity and area view factor calculated for processes 1 (Reference) and 3.

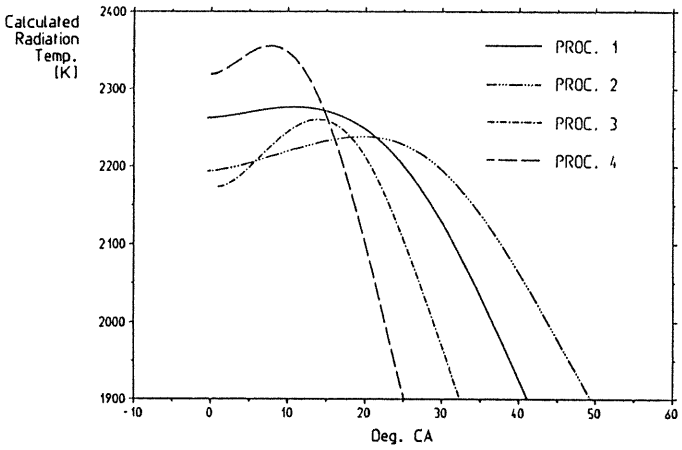

Fig. 2: Calculated radiation temperatures for all four operating conditions (Processes 1 through 4)

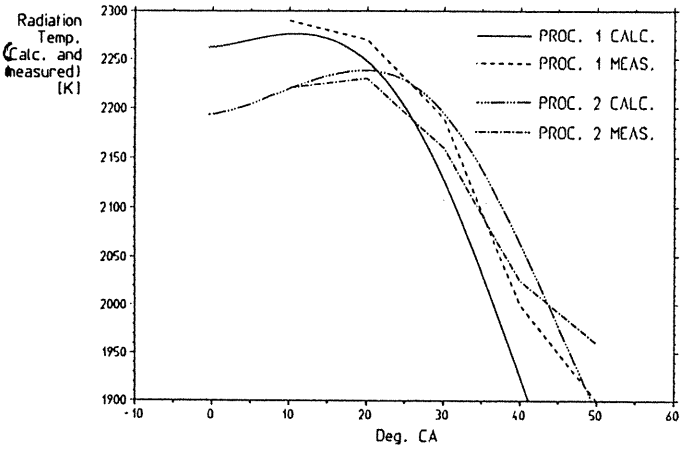

Fig. 3: Comparison between calculated and measured radiation temperatures for processes 1 (Reference) and 2

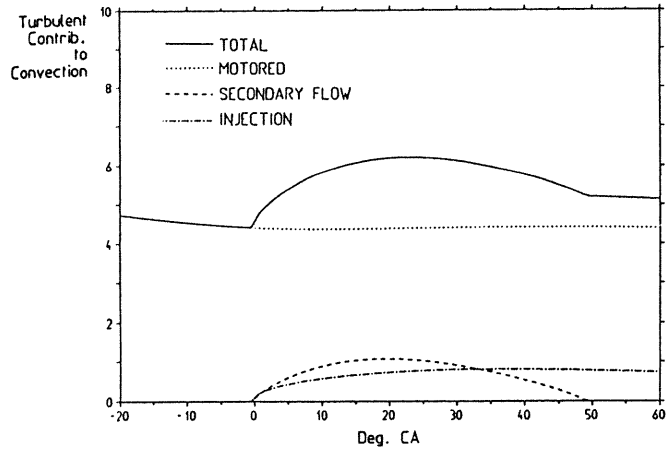

Fig. 4: Contribution of each turbulence generator to convection (Eqs. (21) through (24)) for process 1 (Reference)

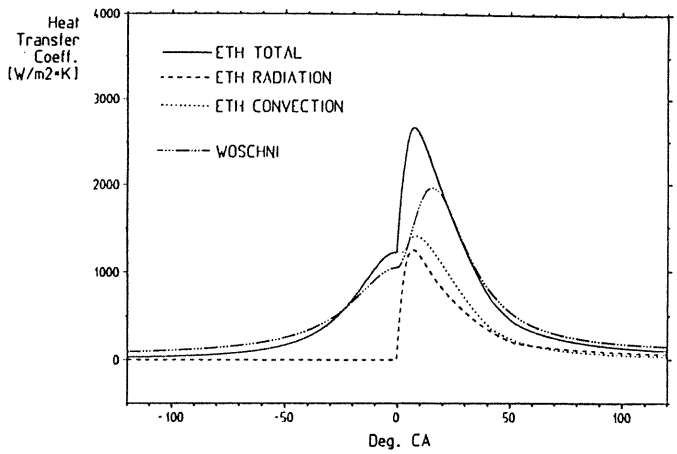

Fig. 7: Heat transfer coefficient according to Woschni (scaled for matching energy balance results) and to ETH-model

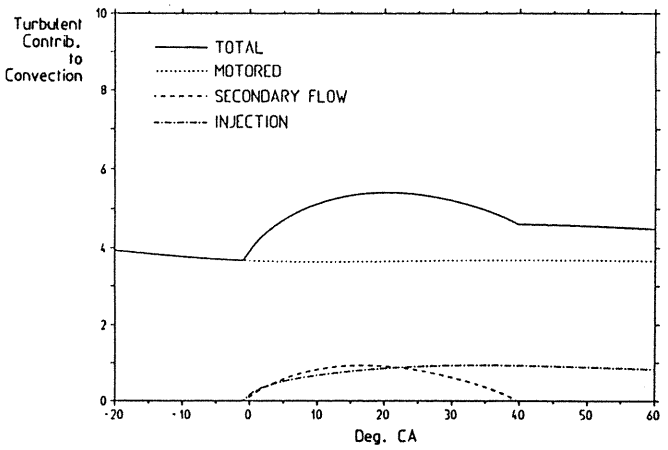

Fig. 5 Contribution of each turbulence generator to convection for operating condition 3

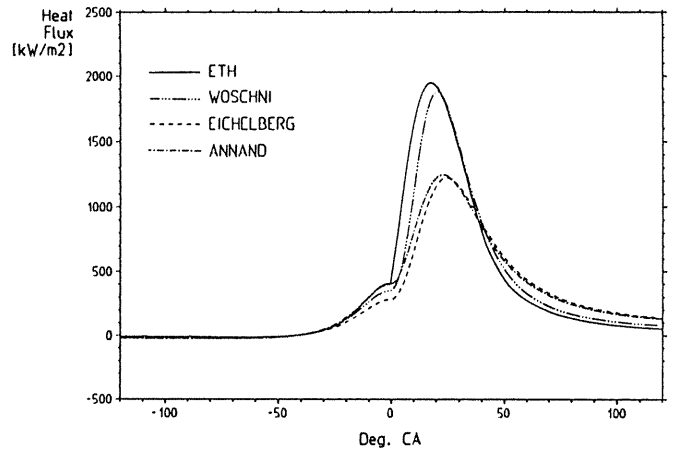

Fig. 8: Comparison of total heat flux between different models scaled for matching energy balance results for process 1 (Reference)

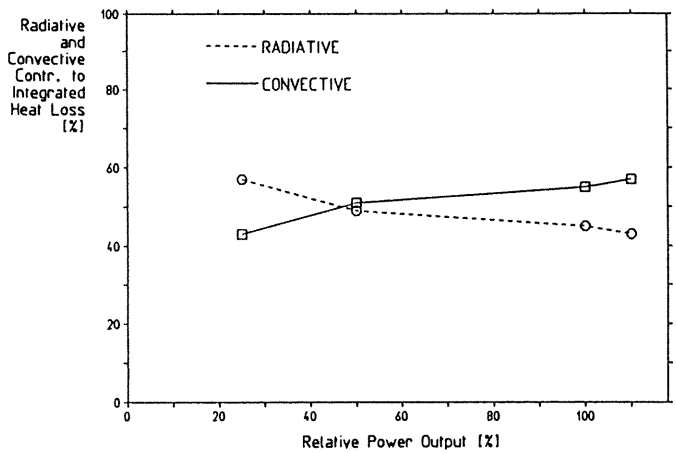

Fig. 6: Relative contributions of radiation and convection for all operating conditions

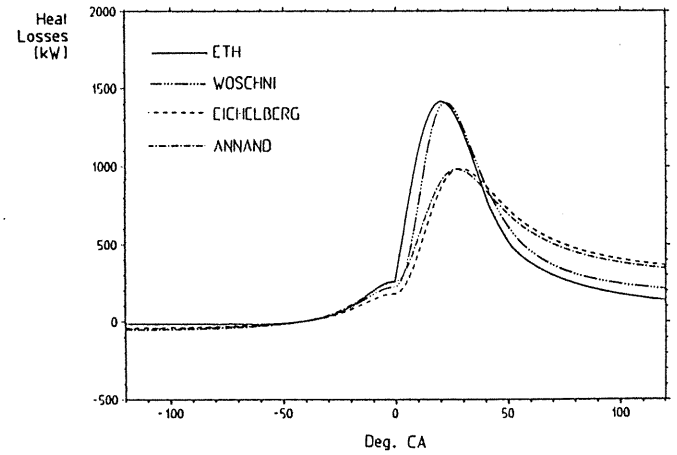

Fig. 9: Comparison of total heat losses between different models scaled for matching energy balance results for process 1 (Reference)

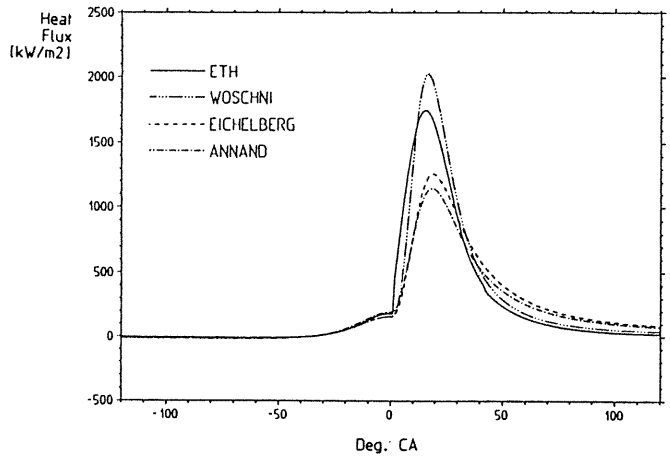

Fig. 10: Comparison of total heat flux between different models for process 3

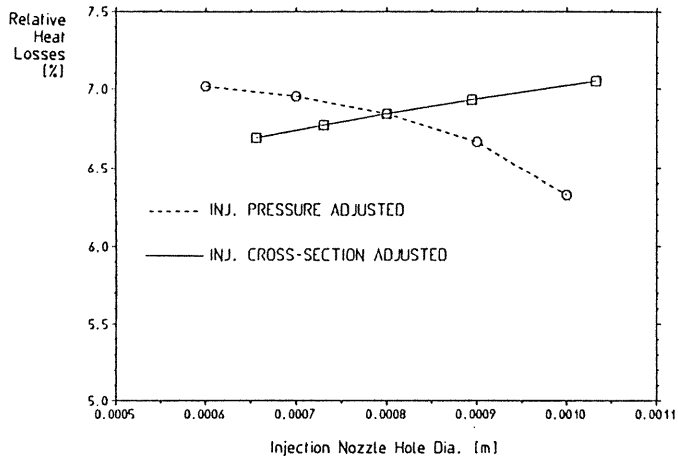

Fig. 13: Influence of Injection Nozzle Hole Diameter on heat losses relative to fuel energy for constant injection duration (Reference process)

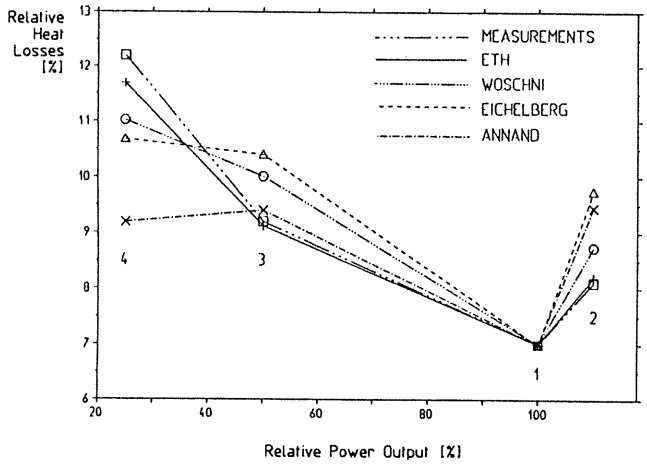

Fig. 11: Heat losses relative to fuel energy for different models in comparison with measurements for all operating conditions (Process 2 is shifted to the right for better visualization)

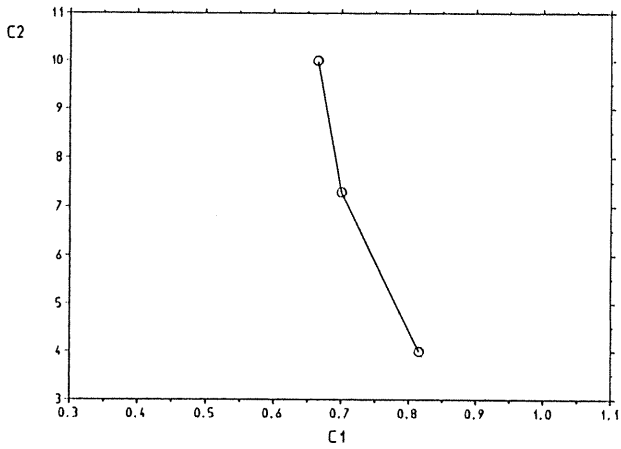

Fig. 14: Mutual interdependence of radiation (area view factor) constants for the same resulting heat flux

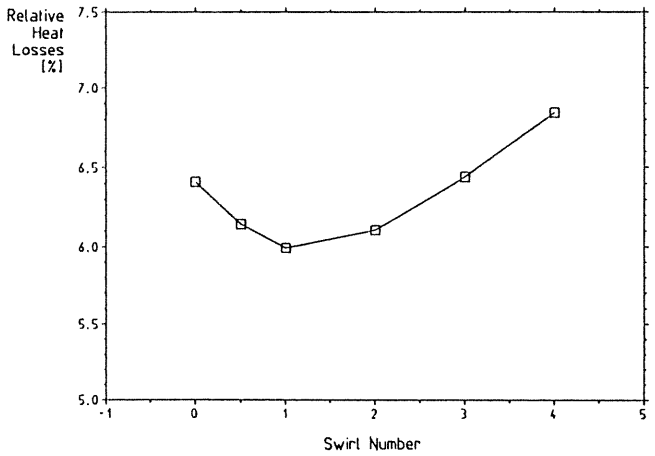

Fig. 12: Prediction of swirl influence on heat losses relative to fuel energy

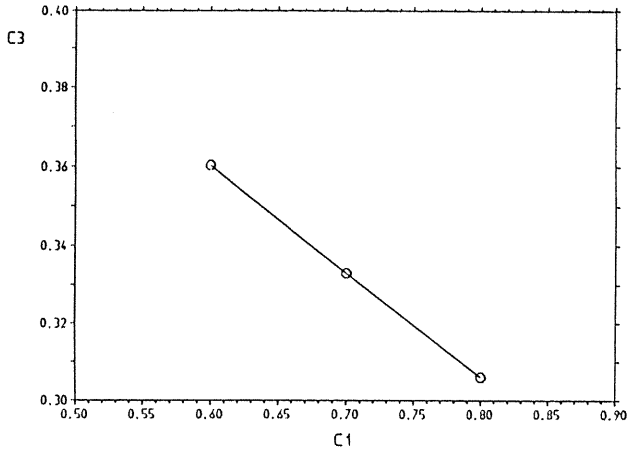

Fig. 15: Mutual interdependence of radiation (C_1) and convection (C_3) constants for the same resulting total heat flux